Supporting Information

Rivera-Molina and Novick 10.1073/pnas.0906536106

SI Methods

Strains and Plasmids. Genotypes of yeast strains used on this work are listed in Table S1. For yeast 2-hybrid analysis, we co-transformed (1) the AH109 strain with plasmids expressing the *GAL4* DNA binding domain (pAS2–1; *TRP1* marker) and the plasmids expressing the *GAL4* activator domain (pACT2; *LEU2* marker). The *GYP1* ORF was PCR-amplified from genomic DNA and cloned into pACT2 as a NcoI–BamHI fragment (NRB1313). In addition to the NcoI site added to the *GYP1* ORF, 2 extra nucleotides (TA) were added before the start codon to clone *GYP1* in-frame with the activator domain. The *HA-YPT1* was amplified from the NRB829 plasmid with 2 extra nucleotides (TA) before the start codon, and cloned as a BamHI-SalI fragment into pAS2–1 (NRB1316). The *YPT1-Q67L* allele was amplified from SFNB891 and cloned the same way into pAS2–1 (NRB1317). *YPT31* ORF was amplified from genomic with 2 extra nucleotides (TA) before start codon, and cloned as a BamHI-SalI into pAS2–1 (NRB1436). The *YPT31-Q72L* allele was generated by site directed mutagenesis on the plasmid mentioned previously (NRB1437).

The *HA-GYP1*, *HA-N-GYP1*, and *C-GYP1* fragments cloned into pGEX4T were amplified from NRB1313 and cloned as BamHI-SalI fragments (NRB1319, NRB1320, NRB1321).

To generate the GFP-*GYP1* and GFP-C-*GYP1* (NRB1322, NRB1323) plasmids, the *ADH1* promoter and *CYC1* terminator cassette were sub-cloned from p416ADH (2) as a SacI-KpnI fragment into pRS306 (*URA3*). *HA-GYP1* and *C-GYP1* fragments were sub-cloned from NRB1319 and NRB1321 into pRS306-pADH-CYC1ter as BamHI-SalI fragments. GFP was cloned as an XbaI-BamHI fragment. These constructs were integrated into the *ura3* locus of strains by digesting the plasmid with PstI. To generate NRB1325 the *HA-GYP1* fragment of NRB1322 was replaced with the *YPT32* ORF amplified from genomic DNA as a BamHI-SalI. This construct was also integrated into the *ura3* locus.

To generate NRB1324 the *HA-GYP1-CYC1term* fragment from NRB1322 was sub-cloned into YIplac128 (3) (*LEU2*) vector as an XbaI-KpnI fragment. The *ADH1* promoter was amplified from genomic DNA (1.5 kb upstream *ADH1* start codon) and cloned as a PstI-XbaI fragment. The mCherry sequence was amplified and cloned as an XbaI-BamHI fragment. This construct was integrated into the *leu2* locus of different strains by digesting the plasmid with AflII. To generate NRB1326, we replaced the *HA-GYP1* from NRB1324 with the *YPT1* ORF amplified from genomic DNA as a BamHI-SalI fragment. This construct was also integrated into the *leu2* locus.

For the co-localization experiments between mCherry-Gyp1p (CH-Gyp1p) and GFP-Ypt32p or mCherry-Ypt1p, we used yeast strains in which the endogenous *GYP1* gene was deleted and replaced with the KanMX marker (NY2769), making the fluorescently tagged Gyp1p the sole copy of *GYP1*.

The NRB1348 construct was generated by amplifying from genomic DNA the 1-kb fragment upstream of the *COG3* stop codon, and cloned it into pRS303 (*HIS3*) as an XhoI-BamHI. This fragment was cloned in-frame with the *3x-GFP-ADH1term* cassette that was cloned into pRS303 as BamHI-NotI fragment. The construct was integrated into the C*OG3* locus by digesting the plasmid with SpeI.

In Vitro Binding Assay. GST-Gyps and 6×-HIS GTPases constructs were expressed and purified from *Escherichia coli* strain BL21 (DE3). GST purified proteins bound to glutathione Sepharose beads or 6×-HIS eluted from Ni-beads were run on SDS/PAGE and stained with Coomassie blue. Densitometry analysis of the stained gel and a BSA-standard was used to estimate the concentration of the full-length purified proteins. Protocols and buffers for the loading of purified 6×-HIS-GTPase proteins with GTPγS and for the binding reactions were described previously (4, 5). The final concentration of GST-Gyps and 6×-HIS GTPases in the binding reaction was approximately 150 nM. After 1 h incubation at room temperature, beads were washed 3 times with binding buffer and were resuspended in 2× loading buffer and boiled for 5 min, and half of the eluted protein was used for SDS/PAGE, transferred to nitrocellulose, and immunoblotted using antibody against each of the GTPases.

Description of Fluorescent Image Acquisition and Digital Enhancement. This supplementary section describes how the fluorescent images for each figure were acquired and how the images were digitally enhanced before analysis. All fluorescent images were handled and enhanced using MacBiophotonics ImageJ. Each list describes the percentage of maximum laser power, the exposure time, the electron multiplier setting, and the linear and non-linear digital filters from the ImageJ software that were used.

For Fig. 2 *A* and *B*, at 488 nm, laser power was 20% and exposure was 75 msec. The electron multiplier was set to 197. Digital enhancement was as follows: remove background from region of interest (ROI), set Gaussian blur filter at 1.5 radius, maximum intensity projection at 4 z-slices, γ filter at 2.

For Fig. 3*A*, at 488 nm, laser power was 30% and exposure was 75 msec. At 568 nm, laser power was 75%, exposure was 400 msec, and the electron multiplier was set at 197. Digital enhancement was as follows: remove background from ROI, Gaussian blur filter at 1.5 radius, maximum intensity projection at 4 z-slices. Spot enhancement 2D filter was set at 2 pixels. Image was converted from 32-bit to 8-bit grayscale, background was removed from ROI, brightness and contrast were adjusted. Minimum GFP images was set at 50, maximum was 180. Minimum mCherry images was set at 50, maximum was 180.

For Fig. 3*B*, at 488 nm, laser power was 35% and exposure was 75 msec. At 568 nm, laser power was 35% and exposure was 75 msec; electron multiplier was set at 197, and digital enhancement was the same as described for Fig. 3*A*.

For Fig. 3 *D* and *E*, at 488 nm, laser power was 35% and exposure was 75 msec. At 568 nm, laser power was 40% and exposure was 75 msec; the electron multiplier was set at 197; and digital enhancement was the same as described for Fig. 3*A*.

For Fig. S5, at 488 nm, laser power was 30% and exposure was 150 msec. At 568 nm, laser power was 80% and exposure was 250 msec. Electron multiplier was set at 197. Digital enhancement was as follows: background was removed from ROI, Gaussian blur filter was set at 1.5 radius; maximum intensity projection at 4 z-slices; spot enhancement 2D filter was set at 2 pixels. The image was converted from 32-bit to 8-bit grayscale and background was removed from ROI, and brightness and contrast were adjusted. Minimum GFP images was set at 25 and maximum was 215. Minimum DsRed images was set at 15 and maximum was 225.

For Fig. 4 and the SI Movies, at 488 nm, laser power was 30% and exposure was 50 msec. At 568 nm, laser power was 45% and exposure was 50 msec. Electron multiplier was set to 197. Digital enhancement was as follows: background was removed from ROI, spot enhancement 2D filter was 2 pixels, images were converted from 32-bit to 8-bit grayscale, 3D hybrid median filter was used; background was removed from ROI and brightness

and contrast were adjusted. Minimum GFP images was set at 50, maximum was 225. Minimum mCherry images was set at 80 and maximum was 245.

Imaris 3D Visualization, Co-Localization, and Generation of Surfaces for Quantification. Enhanced images of cells expressing mCherry-Ypt1p and GFP-Ypt32p were up-loaded into Imaris (Bitplane). The pixel sizes for 3D visualization were 87 nm on the x-y axes and 160 nm on the *z* axis. The square grid around the images has a major thick mark at 0.5 μm. The cell outline was drawn manually based on the bright field image captured for each cell. The co-localization function of Imaris was used to detect co-localized pixels above a minimum threshold setup of 5 on a pixel scatter-plot for each channel. The co-localized pixels were colored white and used to generate a co-localization channel. Each channel (magenta, CH-Ypt1p; cyan, GFP-Ypt32p; and white, co-localization) were used to generate the 3D surfaces. Three-dimensional surfaces represent an outline for pixels the software grouped together based on the following parameters: grain size of 0.085 μm, maximum diameter of 0.700 μm, minimum threshold of 10, and a minimal sum of the pixels intensities of 850 a.u. The software assigns an identification number to each of the surfaces generated. The identification number of a particular surface during the different time points allowed us to extract the signal intensity of each channel (sum intensity Ch1 and Ch2) for any particular surface from Excel spreadsheets generated by the software. These signals were added and used to calculate the percent of total signal for each protein at different time points. In addition, the software quantifies the number of surfaces per frame for each channel. These numbers were averaged for the length of the whole movie (160 frames) to obtain the average number of spots per frame. From the 6 movies generated, we analyzed the change in CH-Ypt1p/GFP-Ypt32p signals for the CH-Ypt1p surfaces that were observed on the first frame of each movie. A surface was analyzed if it lasted more than 5 consecutive frames, and if the surface could be distinguished from any other surface during the analysis.

1. Gietz R, Schiestl R, Willems A, Woods R (1995) Studies on the transformation of intact yeast cells by the LiAc/SS-DNA/PEG procedure. *Yeast* 11:355–360.
2. Mumberg D, Müller R, Funk M (1995) Yeast vectors for the controlled expression of heterologous proteins in different genetic backgrounds. *Gene* 156:119–122.
3. Gietz R, Sugino A (1988) New yeast-Escherichia coli shuttle vectors constructed with in vitro mutagenized yeast genes lacking six-base pair restriction sites. *Gene* 74:527–534.
4. Ortiz D, Medkova M, Walch-Solimena C, Novick P (2002) Ypt32 recruits the Sec4p guanine nucleotide exchange factor, Sec2p, to secretory vesicles; evidence for a Rab cascade in yeast. *J Cell Biol* 157:1005–1015.
5. Du L, Novick P (2001) Purification and properties of a GTPase-activating protein for yeast Rab GTPases. *Methods Enzymol* 329:91–99.
6. Losev E, et al. (2006) Golgi maturation visualized in living yeast. *Nature* 441:1002–1006.

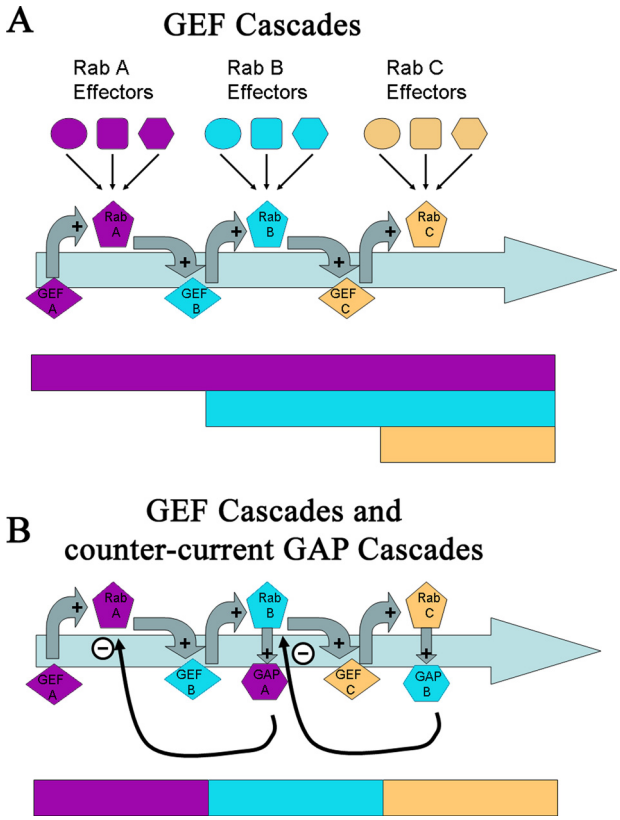

Fig. S1. Model illustrating how GEF and GAP cascades establish Rab boundaries along a membrane traffic pathway. (*A*) GEF cascades: a simple illustration of the GEF cascade model and how it can establish the sequential activation of Rabs (Rab A recruits GEF B, Rab B recruits GEF C). Color-coded horizontal bars (*Lower*) showing how Rabs (and hence their effectors) will become inter-mixed on membranes by this mechanism. (*B*) GEF cascades and countercurrent GAP cascades: the same illustration as *A*, but with the addition of a countercurrent GAP cascade mechanism (Rab B recruits GAP A, Rab C recruits GAP B). Color-coded bar (*Lower*) postulating how the addition of the GAP cascades will reduce the inter-mixing of Rabs and promote the specific localization of their effectors along the pathway.

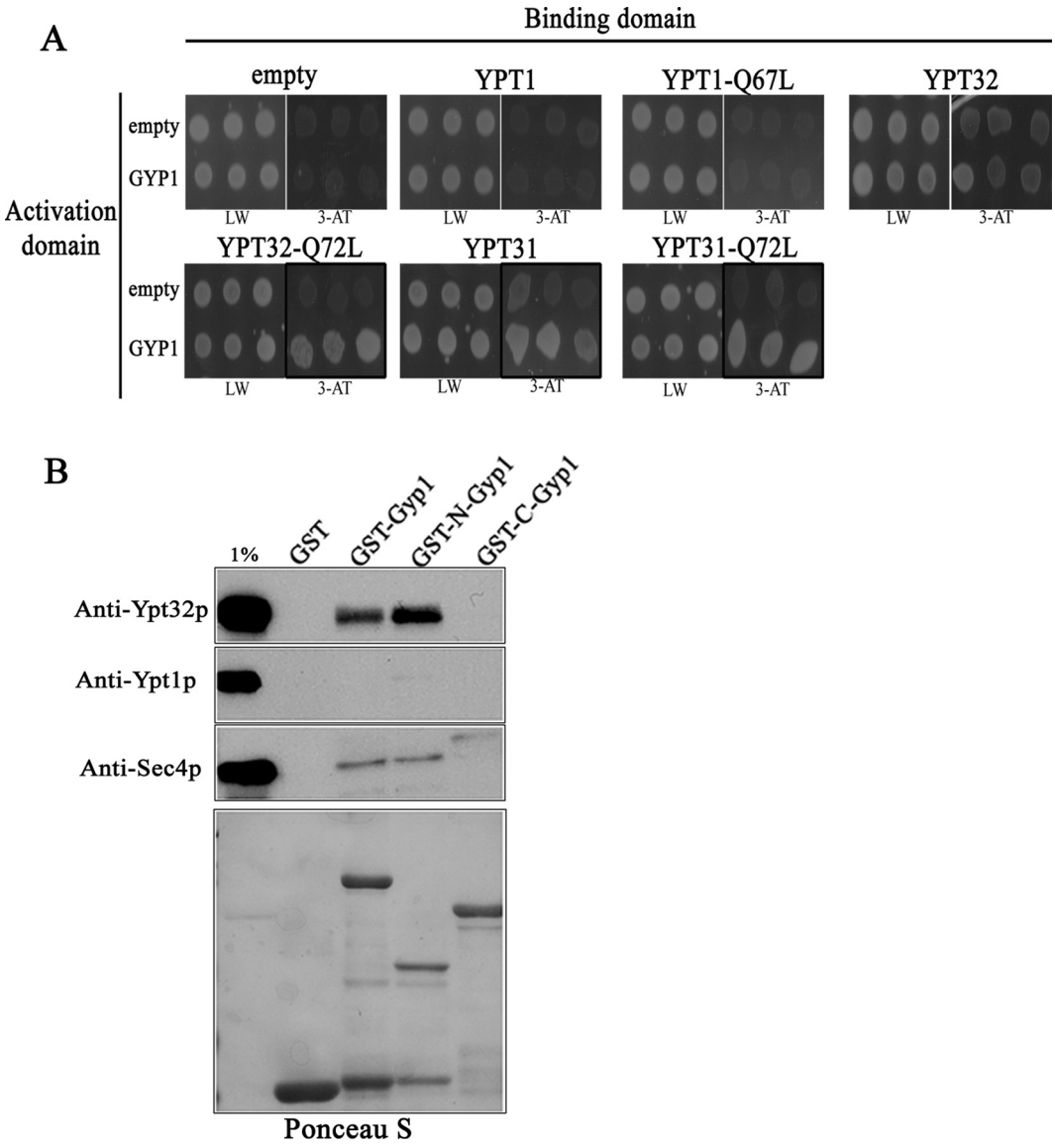

Fig. S2. Gyp1p interacts with active Ypt31p by yeast 2-hybrid assay and with Ypt32-GTPγS by in vitro binding experiments. (*A*) A yeast 2-two hybrid assay between *GYP1* and *YPT1*, *YPT32*, and *YPT31* or the hydrolysis-deficient allele of each YPT. Growth on solid medium lacking leucine/tryptophan (*LW*) indicates the presence of the plasmids, growth on solid medium lacking leucine/tryptophan/histidine + 10 mM 3-AT medium (*3-AT*) indicates a positive 2-hybrid interaction. (*B*) Bacterially purified Ypt32p, Ypt1p, or Sec4p were preloaded with GTPγS and incubated with the various GST-Gyp1 fusion proteins shown in Fig. 1*C*. Binding was detected by Western blot using antibodies specific to each GTPase. Ponceau S staining of one of the membranes shows the presence of the various GST-Gyp constructs on the beads used for the binding reactions.

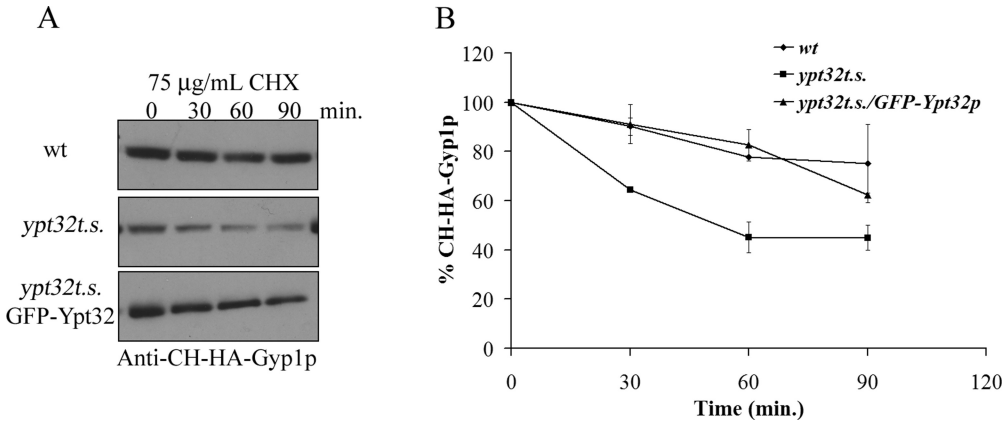

Fig. S3. A functional Ytp32p is important for the stability of Gyp1p. (*A*) WT (NY2775), *ypt32t.s.* (NY2776), or *ypt32t.s.*/GFP-Ypt32p (NY2777) cells expressing the mCherry-HA-Gyp1p (CH-HA-Gyp1p) were incubated in media containing cycloheximide, and every 30 min an equivalent amount of culture was removed and protein extracts were prepared. An equal volume of sample per time point was used to detect the levels of CH-HA-Gyp1p by Western blot with an antibody against mCherry before and after the treatment with cycloheximide. (*B*) Line graph showing the changes in CH-Gyp1p levels after cycloheximide treatment. CH-Gyp1p levels were determined by densitometry analysis. The signal of CH-Gyp1p at time 0 was established as the 100% signal for each of the strains. After 60 min the *ypt32t.s.* strain showed a 50% reduction of CH-Gyp1p levels, which was not observed in WT or *ypt32t.s.*/GFP-Ypt32p cells.

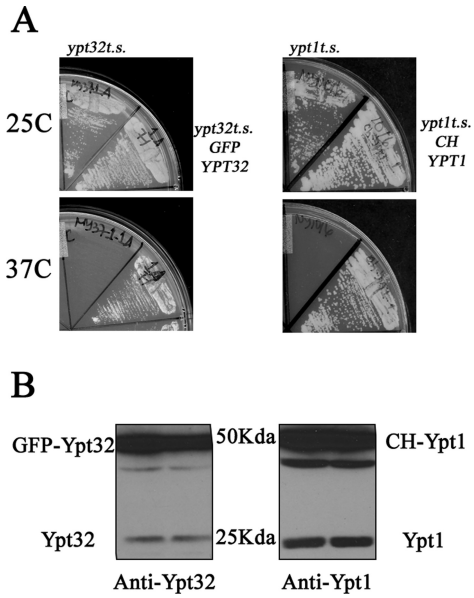

Fig. S4. Functionality and protein levels of GFP-Ypt32p and mCherry-Ypt1p. (*A*) Rescue of *ytp32t.s.* (NY2770) or *ypt1t.s.* (NY1016) growth at 37 °C by expression of GFP-YTP32 (NY2771) or mCherry-YPT1 (CH-YPT1; NY2786), respectively. (*B*) Western blot to demonstrate the level of over-expression of GFP-Ypt32p or CH-Ypt1p in comparison with endogenous levels in WT cells total protein lysates. GFP-Ypt32p was 10 to 12 fold higher than endogenous Ypt32p, and CH-Ypt1p was 4 to 5 fold higher than endogenous Ypt1p.

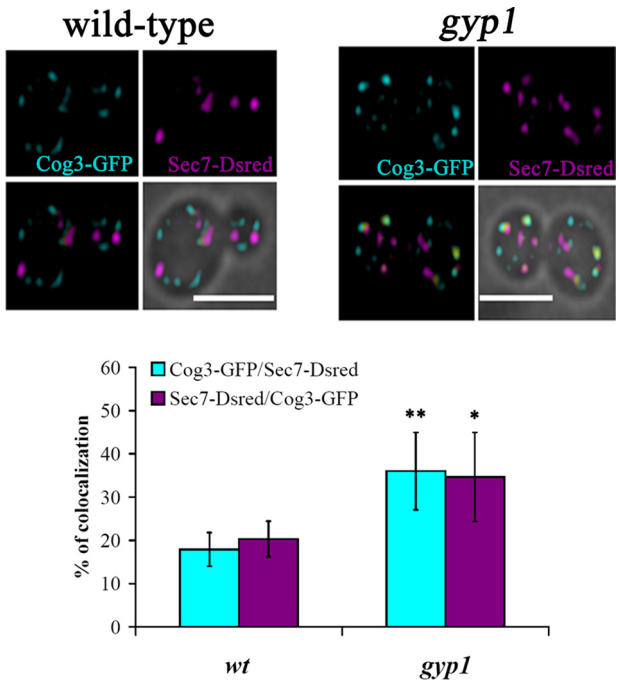

Fig. S5. The *gyp1* strain showed an increased co-localization of Cog3p and Sec7p. Fluorescent images of WT (NY2947) and *gyp1* (NY2948) cells expressing Cog3p-3xGFP and Sec7p-6x-DsRed. Merged fluorescent images were superimposed with the bright-field image (*Lower Right*) to show the cell contour. Bar graph shows the percentage of co-localization of the following proteins: Cog3p-3xGFP spots containing Sec7p-6xDsRed signal (cyan bar), Sec7p-6xDsRed spots containing Cog3p-3xGFP signal (magenta bar). Approximately 100 cells, 2–5 spots/cell, error bar indicates SD; $**P < 0.001$; $*P < 0.006$, (*t* test) between WT and *gyp1*. (Scale bar, 5 μm.)

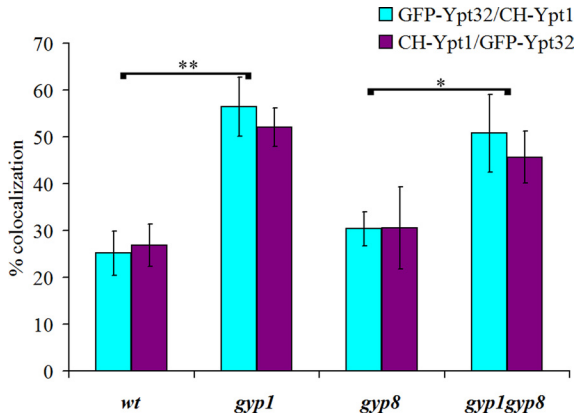

Fig. S6. The *gyp8* strain did not show increased co-localization of mCherry-Ypt1p and GFP-Ypt32p. Bar graph showing the percentage of compartments in which GFP-Ypt32p and CH-Ypt1p (cyan bars) co-localize, or the percentage of compartments in which CH-Ypt1p and GFP-Ypt32p (magenta bars) co-localize in WT (NY2780), *gyp1* (NY2781), *gyp8* (NY2784), or *gyp1gyp8* (NY2785) strains (error bars indicate SD). $**P < 0.001$ (*t* test) between WT and *gyp1*; $*P < 0.003$, (*t* test) between *gyp8* and *gyp1gyp8*.

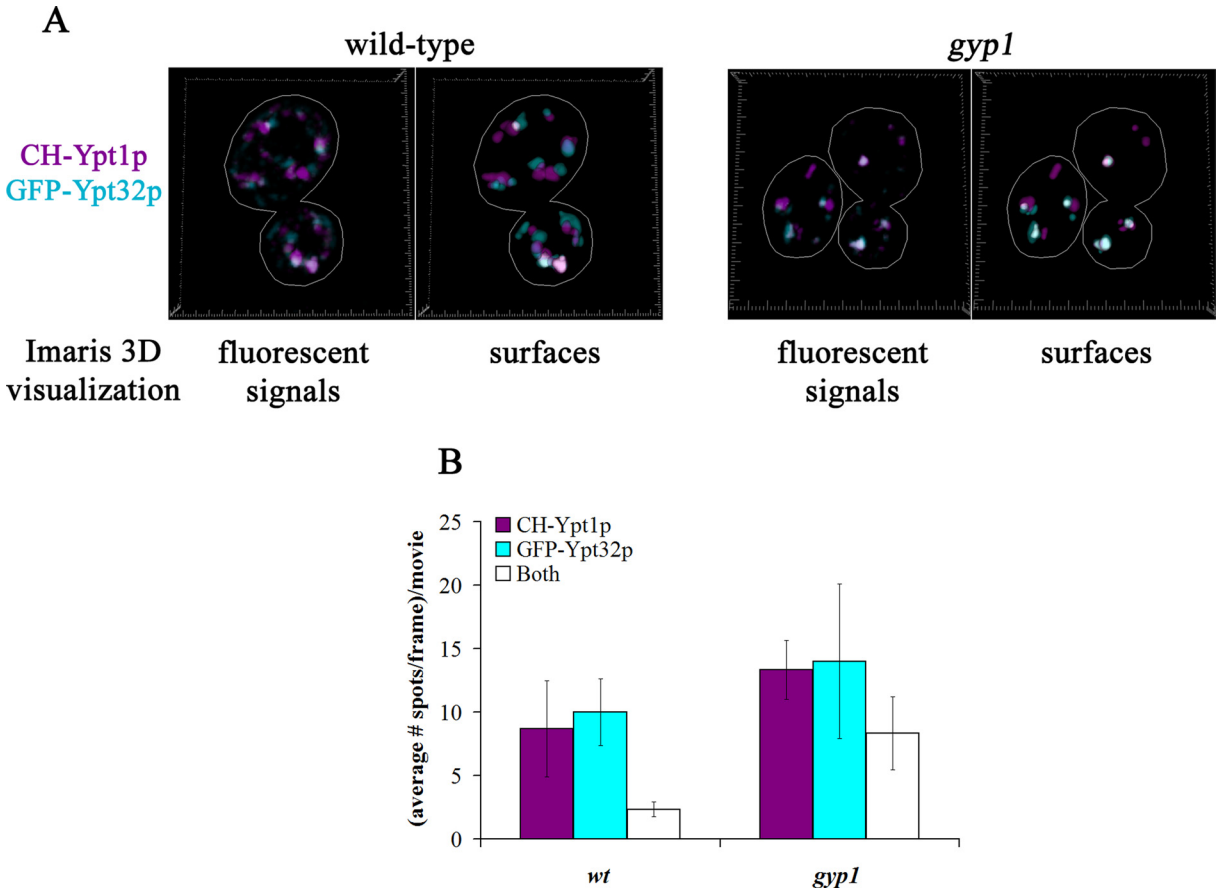

Fig. S7. Conversion of fluorescent signals to surfaces and the quantification of the number of the CH-Ypt1p, GFP-Ypt32p, or co-localized spots in WT and *gyp1* cells movies. (*A*) WT or *gyp1* cells panels showing the merged images of CH-Ypt1p (magenta) and GFP-Ypt32p (cyan) fluorescent signals or the corresponding surfaces visualized with Imaris 3-D software. (*B*) Bar graph shows the quantification of the average number of spots/frame for CH-Ypt1p (magenta), GFP-Ypt32p (cyan), and co-localized (white) on the 3 movies captured for WT and *gyp1* cells (error bars indicate SD).

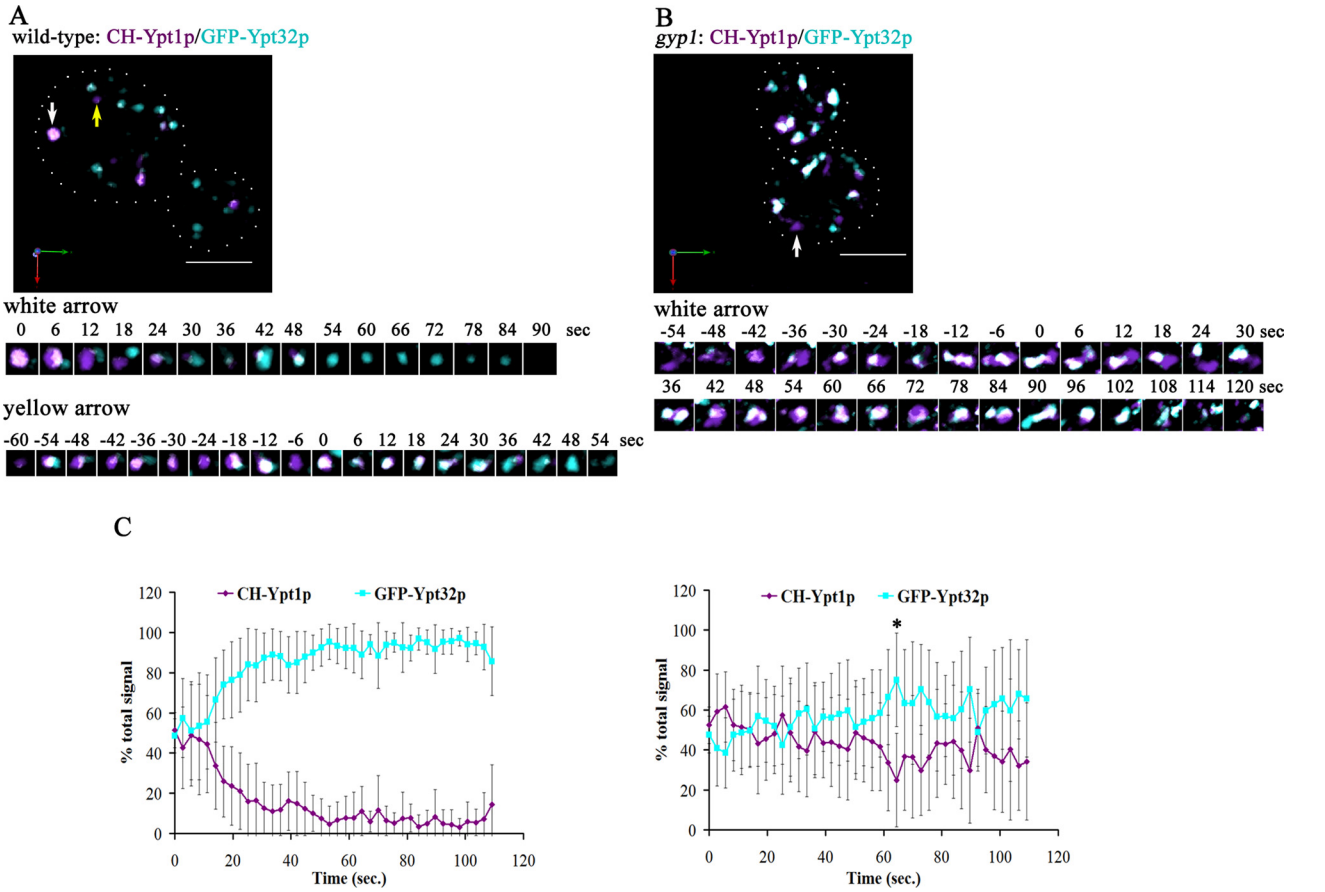

Fig. S8. Conversion of a Ypt1p compartment to a Ypt32p compartment. (*A*) Images from Movie S2 demonstrates the conversion of a CH-Ypt1p compartment to a GFP-Ypt32p compartment (arrows) in WT cells. Cropped images of the compartments labeled with an arrows in *A* during the entire time series are shown (*Lower*). Numbers indicate the time in seconds relative to the frame were the percent of total signal was 50% (i.e., time 0). White spots represent the co-localization between CH-Ypt1p and GFP-Ypt32p. (*B*) Images from Movie S4 demonstrating the conversion of a CH-Ypt1p compartment to a GFP-Ypt32p compartment (arrow) in *gyp1* cells. Cropped images of the compartment labeled with an arrow in *B* during the entire time series are shown (*Lower*). (*C*) Averaged time course of the percent of total signal of CH-Ypt1p and GFP-Ypt32p in WT (*Left*) or *gyp1* (*Right*) cells ($n = 13$, error bars indicate SD); $^*P < 0.002$ (*t* test) between percentages of total signal for Ypt1p and Ypt32p at the particular time point.

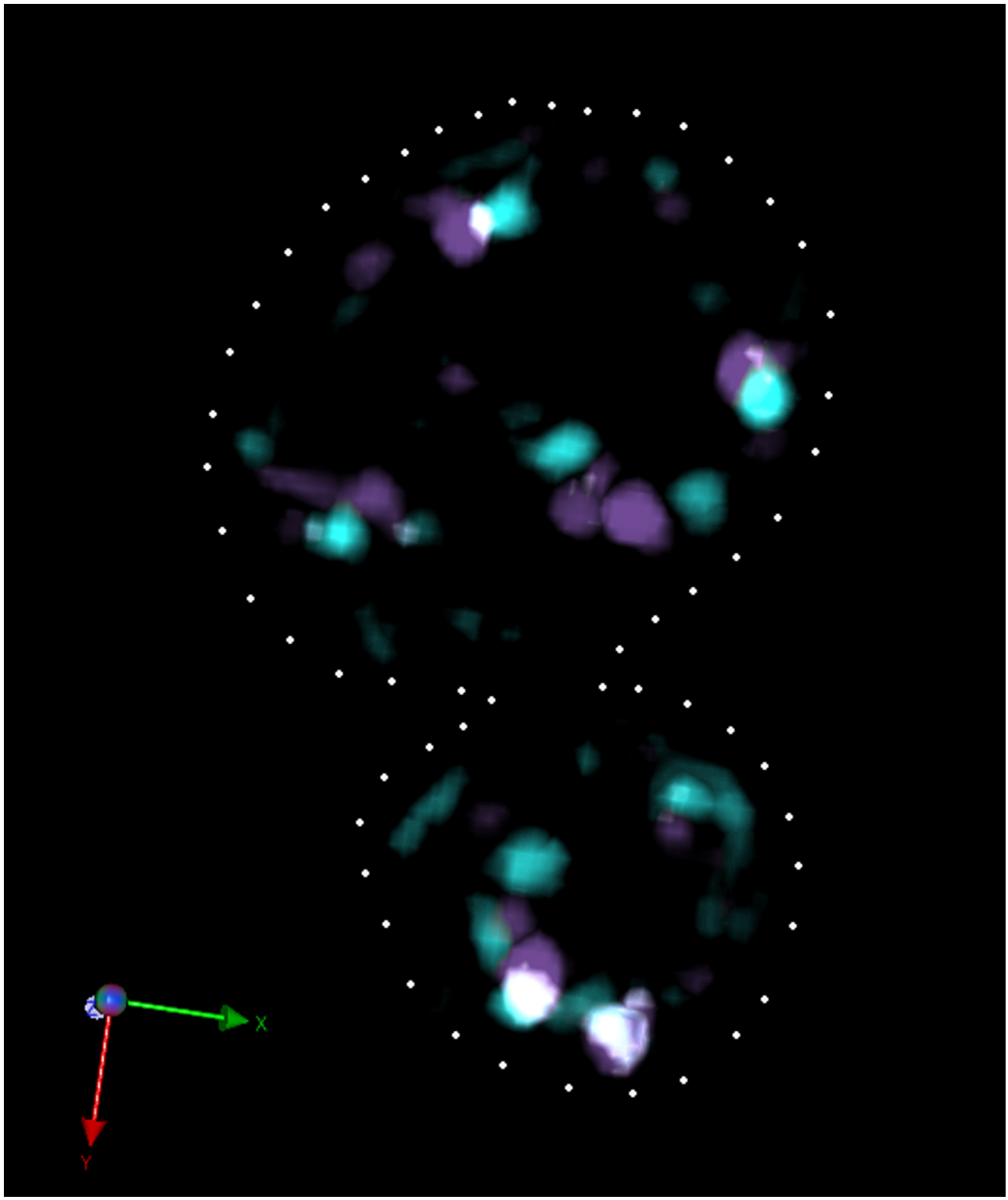

Movie S1. mCherry-Ypt1p to GFP-Ypt32 compartment conversion in the WT cells. The movies show the conversion of mCherry-Ypt1p (magenta) compartments to GFP-Ypt32p (cyan) over time. Co-localization is represented by the white color. Arrow indicates the compartment that was followed.

Movie S1 (AVI)

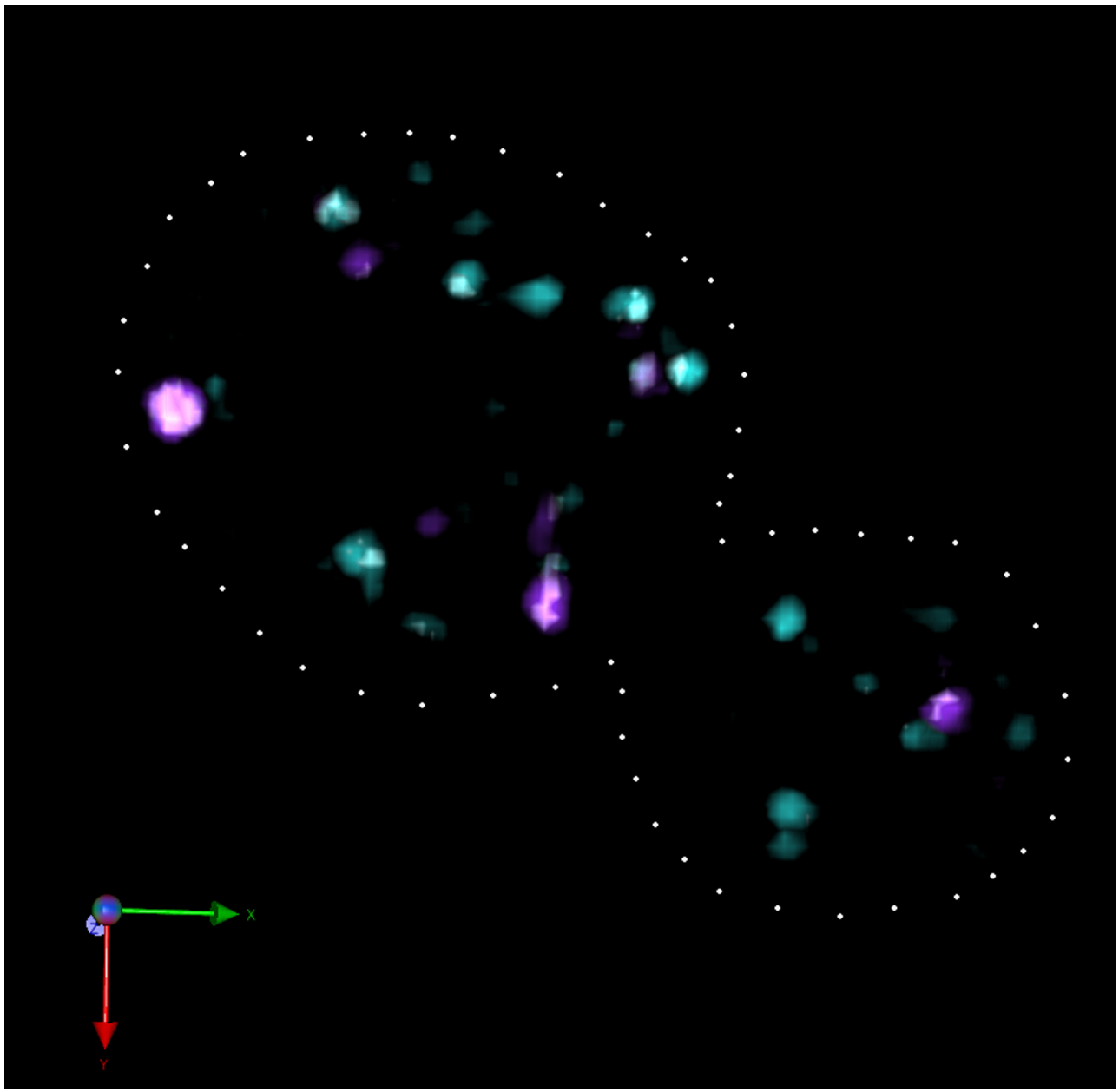

Movie S2. mCherry-Ypt1p to GFP-Ypt32 compartment conversion in the WT cells. The movies show the conversion of mCherry-Ypt1p (magenta) compartments to GFP-Ypt32p (cyan) over time. Co-localization is represented by the white color. Arrow indicates the compartment that was followed.

Movie S2 (AVI)

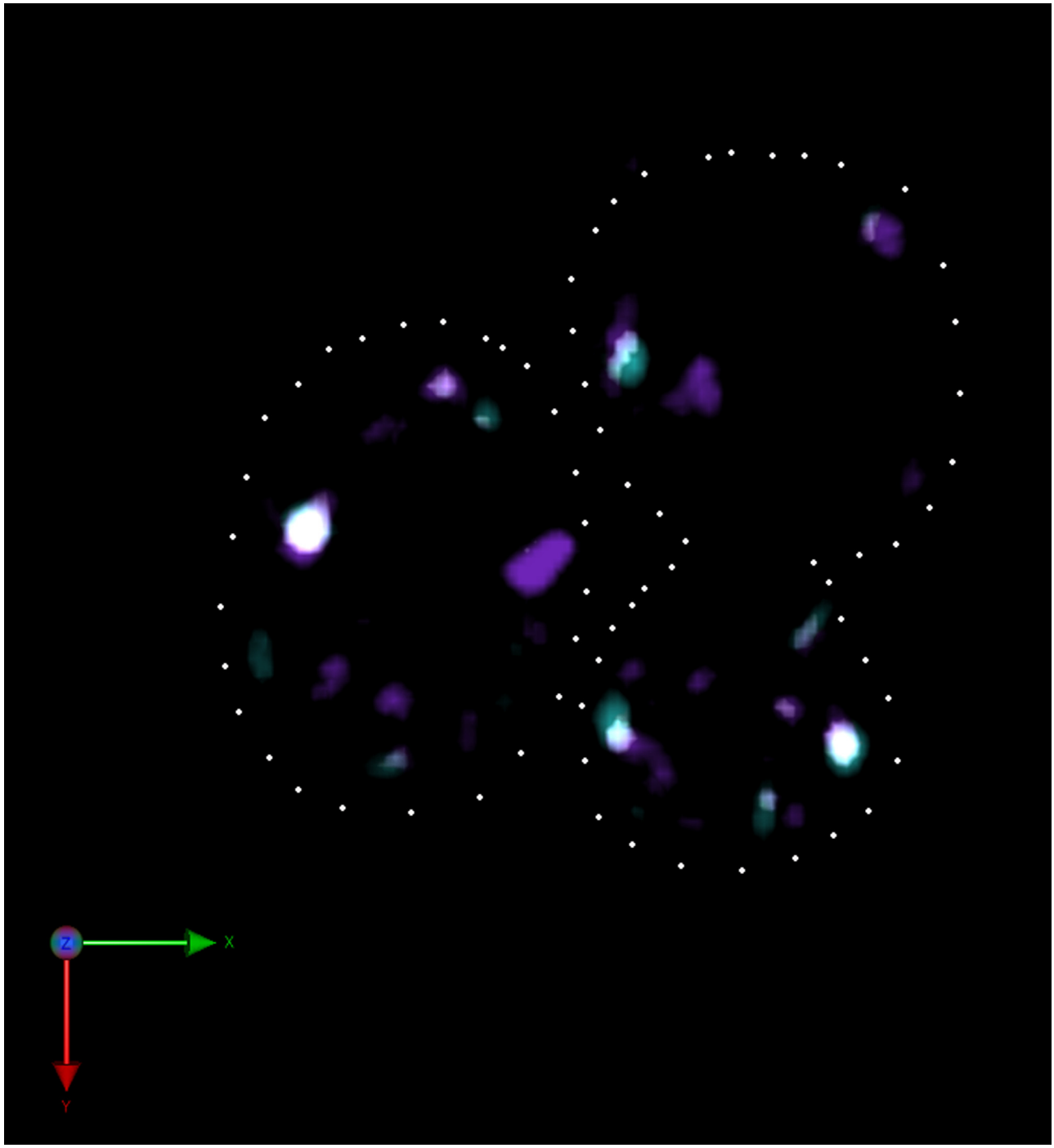

Movie S3. mCherry-Ypt1p to GFP-Ypt32 compartment conversion in a *gyp1* cells. The movies show the conversion of mCherry-Ypt1p (magenta) compartments to GFP-Ypt32p (cyan) over time. Co-localization is represented by the white color. Arrow indicates the compartment that was followed.

Movie S3 (AVI)

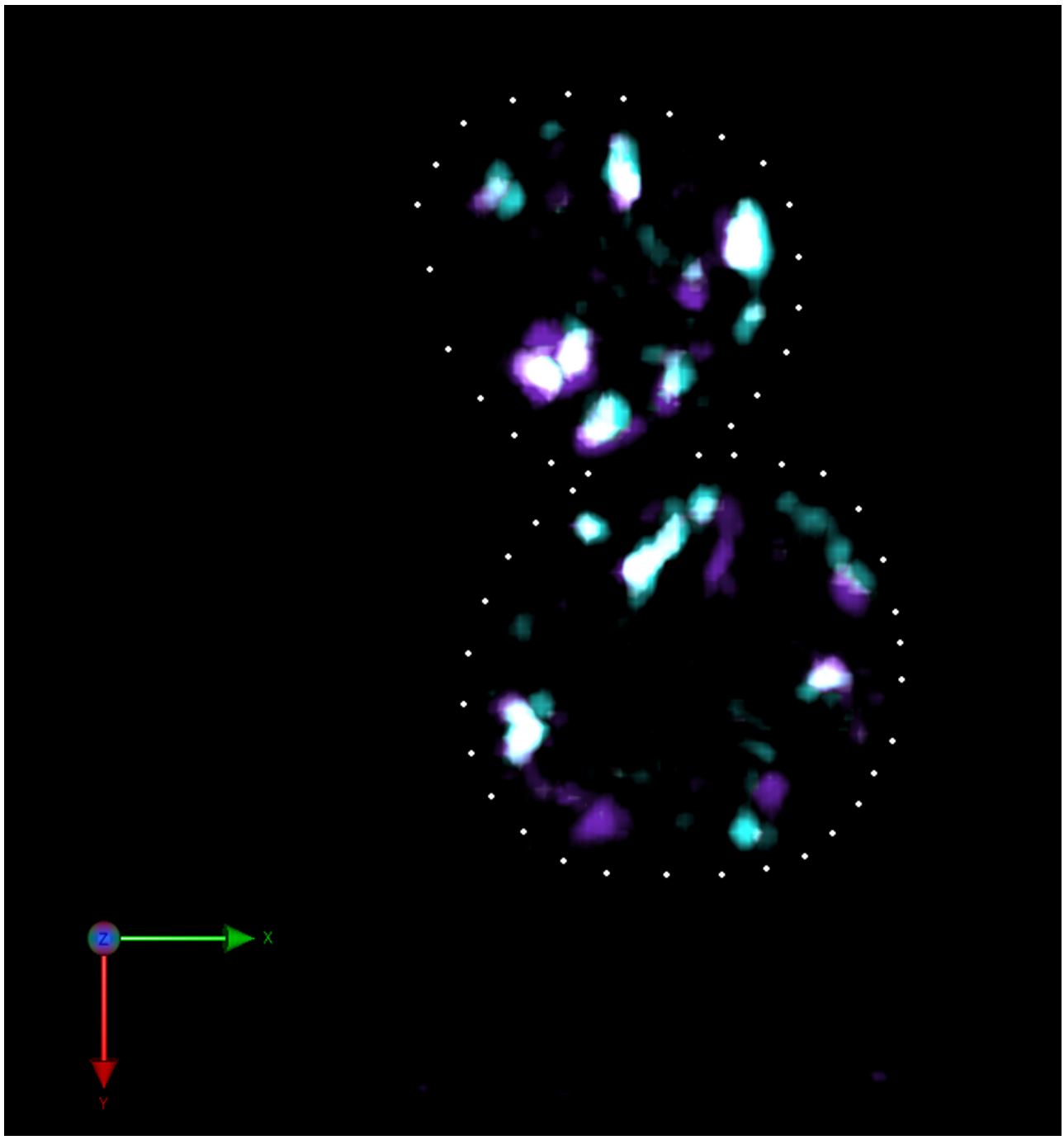

Movie S4. mCherry-Ypt1p to GFP-Ypt32 compartment conversion in a *gyp1* cells. The movies show the conversion of mCherry-Ypt1p (magenta) compartments to GFP-Ypt32p (cyan) over time. Co-localization is represented by the white color. Arrow indicates the compartment that was followed.

Movie S4 (AVI)

Table S1. Genotypes of yeast strains used

Strain	Genotype
NY1211	Mat α GAL+ *ura3–52 leu2–3,112 his3Δ200*
AH109	Mat a *trp1–901 leu2–3, 112 ura3–52 his3–200 gal4D gal80D LYS2::GAL1UAS-GAL1TATA-HIS3 MEL1 GAL2UAS-GAL2TATA-ADE2 URA3::MEL1UAS-MEL1TATA-lacZ*
NY2769	Mat α GAL+ *ura3–52 leu2–3,112 his3Δ200 gyp1Δ::KanMX*
NY2770	Mat α GAL+ *ura3–52:: leu2–3,112 his3Δ200 ypt31Δ::HIS3 ypt32t.s.(A141D)*
NY2771	Mat α GAL+ *ura3–52::URA3:GFP-YPT32 (NRB1325) leu2–3,112 his3Δ200 ypt31Δ::HIS3 ypt32t.s.*
NY2772	Mat α GAL+ *ura3–52::URA3:GFP-HA-GYP1 (NRB1322) leu2–3,112 his3Δ200*
NY2773	Mat α GAL+ *ura3–52::URA3:GFP-HA-GYP1 leu2–3,112 his3Δ200 ypt31Δ::HIS3 ypt32t.s.*
NY2774	Mat α GAL+ *ura3–52::URA3:GFP-C-GYP1 (NRB1323) leu2–3,112 his3Δ200*
NY2775	Mat α GAL+ *ura3–52 leu2–3,112::LEU2:mCherry-HA-GYP1 (NRB1324) his3Δ200*
NY2776	Mat α GAL+ *ura3–52 leu2–3,112::LEU2:mCherry-HA-GYP1 his3Δ200 ypt31Δ::HIS3 ypt32t.s.*
NY2777	Mat α GAL+ *ura3–52::URA3:GFP-YPT32 leu2–3,112::LEU2:mCherry-HA-GYP1 his3Δ200 ypt31Δ::HIS3 ypt32t.s.*
NY2778	Mat α GAL+ *ura3–52::URA3:GFP-YPT32 leu2–3,112::LEU2:mCherry-GYP1 his3Δ200 gyp1Δ::KanMX*
NY2779	Mat α GAL+ *ura3–52::URA3:GFP-HA-GYP1 leu2–3,112::LEU2:mCherry-YPT1 (NRB1326) his3Δ200 gyp1Δ::KanMX*
NY2780	Mat α GAL+ *ura3–52::URA3:GFP-YPT32 leu2–3,112::LEU2:mCherry-YPT1 his3Δ200*
NY2781	Mat α GAL+ *ura3–52::URA3:GFP-YPT32 leu2–3,112::LEU2:mCherry-YPT1 his3Δ200 gyp1Δ::KanMX*
NY2782	Mat α GAL+ *ura3–52 leu2–3,112 his3Δ200 gyp8Δ::HISMX*
NY2783	Mat α GAL+ *ura3–52 leu2–3,112 his3Δ200 gyp1Δ::KanMX gyp8Δ::HISMX*
NY2784	Mat α GAL+ *ura3–52::URA3:GFP-YPT32 leu2–3,112::LEU2:mCherry-YPT1 his3Δ200 gyp8Δ::HISMX*
NY2785	Mat α GAL+ *ura3–52::URA3:GFP-YPT32 leu2–3,112::LEU2:mCherry-YPT1 his3Δ200 gyp1Δ::KanMX gyp8Δ::HISMX*
NY1016	Mat α *ura3–52 leu2–3 ypt1–1t.s.*
NY2786	Mat α *ura3–52 leu2–3::LEU2:mCherry-YPT1 ypt1–1t.s.*
NY2947	Mat α GAL+ *ura3–52 leu2–3,112 his3Δ200 SEC7–6xDsred::URA3 (NRB1337), COG3–3xGFP::HIS3 (NRB1348)*
NY2948	Mat α GAL+ *ura3–52 leu2–3,112 his3Δ200 SEC7–6xDsred::URA3 gyp1Δ::KanMX, SEC7–6xDsred::URA3, COG3–3xGFP::HIS3*

Table S2. Plasmids used

Plasmid	Description
NRB1313	pACT2-GYP1
NRB1314	pAS2–1-YPT32(4)
NRB1315	pAS2–1-YPT32-Q72L(4)
NRB1316	pAS2–1-HA-YPT1
NRB1317	pAS2–1-YPT1-Q67L
NRB1318	pAS2–1-YPT32-S27N(4)
NRB1436	pAS2–1-YPT31
NRB1437	pAS2–1-YPT31-Q72L
NRB1319	pGEX4T-HA-GYP1
NRB1320	pGEX4T-HA-N-GYP1 from 1 to 210 a.a.
NRB1321	pGEX4T-C-GYP1 from 205 to 637 a.a.
NRB1322	pRS306 pADH1-GFP-HA-GYP1-CYC1term (URA3)
NRB1323	pRS306 pADH1-GFP-C-GYP1-CYC1term (URA3)
NRB1324	YIplac128 pADH1-mCherry-HA-GYP1-CYC1term (LEU2)
NRB1325	pRS306 pADH1-GFP-YPT32-CYC1term (URA3)
NRB1326	YIplac128 pADH1-mCherry-YPT1-CYC1term (LEU2)
NRB1337	pSSEC7–6xDsredM1(6) (URA3)
NRB1348	pRS303–3′COG3–3xGFP-ADHter (HIS3)